PTEP

Prog. Theor. Exp. Phys. **2014**, 113D04 (22 pages)
DOI: 10.1093/ptep/ptu135

Gaussian expansion methods under the absorbing boundary condition

Y. Takenaka[1], R. Otani[1], M. Iwasaki[1], K. Mimura[1], and M. Ito[1,2,*]

[1]*Department of Pure and Applied Physics, Kansai University, Yamatecho, 3-3-35, Suita 564-8680, Japan*
[2]*Research Center for Nuclear Physics (RCNP), Osaka University, Mihogaoka 10-1, Suita 567-0047, Japan*
*E-mail: itomk@kansai-u.ac.jp

Received March 7, 2014; Revised August 27, 2014; Accepted September 4, 2014; Published November 24, 2014

We have analyzed the applicability of the various Gaussian bases to the variational calculation under the absorbing boundary condition. Three kinds of Gaussian basis are investigated: shifted, tempered, and oscillating Gaussians. All the basis functions are successful in describing a resonance with a sharp width, but the features of the non-resonant continuum states are very different among the employed Gaussian bases. The energy eigenvalues calculated from the shifted Gaussian show the regular sequence in a complex energy plane, while the energy distribution obtained by the tempered and oscillating Gaussian deviates from the regular distribution. The wave functions in the non-resonant continuum are investigated for the individual Gaussian bases. The shifted Gaussian nicely describes the extensively oscillating feature over a wide spatial range, but the wave functions of the other two bases concentrate around the interaction area. The calculation of the shifted Gaussian and oscillating Gaussian largely reduces the errors contained in the resonance wave function. The trajectories of the resonance, obtained by a variation of the strength of the absorbing potential, are pursued in a complex energy plane. The resonance trajectories for the shifted and oscillating Gaussian bases become stationary around the optimal strength of the absorber, while such a stationary trajectory is not clearly observed in the calculation of the tempered Gaussian. An appropriate combination of the basis functions and the absorbing boundary condition is discussed.

Subject Index D10, D11

1. Introduction

The basis expansion method is one of the most powerful tools in the calculation of few-body quantum systems. For example, the computational techniques of the basis expansion methods have progressed rapidly in few-nucleon systems [1,2], and, therefore, the basis expansion technique has been applied to few-body problems in cold atomic systems [3,4]. Most of the basis expansion methods have been done by employing the Gaussian basis function [1–6]. The so-called tempered Gaussian, having a functional form of $\exp(-\nu r^2)$ [1], is the most widely used in few-body calculations because of its mathematically convenient properties; specifically, the matrix elements on the tempered Gaussian basis can be evaluated in an analytical way in many physical problems. A series of the tempered Gaussian bases is generated by the geometric progression of the width parameter ν. The tempered Gaussian basis especially succeeds in handling the ground and low-lying bound states. In addition, a superposition of the tempered Gaussian basis can describe not only tightly bound systems but also weakly bound systems, in which a tail of the wave function is largely extended due to the quantum

tunneling effect. Thus, the tempered Gaussian basis is one of the standard trial functions in the basis expansion method.

In contrast, current research in few-body problems is extended to unbound continuum states above the particle threshold, and the dynamics of few-body resonances have been extensively explored. In a naive treatment of the unbound states, a scattering boundary condition should be imposed among the interacting particles, but imposing the scattering boundary condition for a few particles is complicated in general. In particular, the exact treatment of the few-body scattering state requires special techniques for the long-range interaction, such as the Coulomb force. In order to avoid the complexity of the few-body scattering boundary condition, the scattering problem is often reduced to the bound-state-like problem by transforming the Hamiltonian of a total system into a non-Hermite form. There are two representative methods of the non-Hermitian transformations: the complex scaling method (CSM) [6–14] and the method of the absorbing boundary condition (ABC), or the method of the complex absorbing potential (CAP) [15–24].

In CSM [6–14], the coordinates of the position ($\mathbf{r}$) and the momentum ($\mathbf{k}$), contained in the original Hamiltonian $H(\mathbf{r}, \mathbf{k})$, are simply scaled as $\mathbf{r} \to \mathbf{r}e^{i\theta}$ and $\mathbf{k} \to \mathbf{k}e^{-i\theta}$. A wave function of a resonant state originally diverges at an asymptotic region, but this diverging tail is transformed into the damping form by the scaling for the coordinates. Since an amplitude of a scaled wave function is damped at an asymptotic region, the scaled solutions can be obtained by the basis expansion technique, in a similar manner to the bound-state problem. CSM is one of the most useful tools in handling the few-body continuum; however, there are two limitations in its application. First, at the very least, an explicit functional form of the total Hamiltonian must be obtained. This means that the CSM is difficult to apply if we know only the matrix elements of the Hamiltonian instead of the Hamiltonian itself. Secondly, there are some restrictions in the functional form of an employed interaction. If the interaction cannot keep its analytic property for the complex scaling, a singularity appears in the scaled equation, and the CSM calculation breaks down.

The other method for the resonant and continuum states is the absorbing boundary condition (ABC) [15–24]. In this method, the negative imaginary (or complex) potential is placed at the interaction-free region of the total system. The diverging tail of the resonant wave function is absorbed by the outer imaginary potential, leading to the damping behavior of the resonant wave function at an asymptotic region. Thus, the basis expansion method can be applied under ABC. In ABC, an absorber is introduced in addition to an original Hamiltonian, and the matrix elements of the original Hamiltonian are invariant with respect to the introduction of the absorber. Therefore, there is no restriction in the functional form of interactions. Furthermore, in ABC, we need only the matrix elements of the original Hamiltonian even if an explicit functional form of the original Hamiltonian is unclear. This is one of the advantages of ABC in marked contrast to CSM. In fact, we encounter such a situation in the microscopic cluster model, the generator coordinate method (GCM) [5], in which only the matrix elements of the Hamiltonian are numerically evaluated. The ABC method works nicely in the framework of GCM [20,21].

In recent studies, CSM has been applied to three-body nuclear systems, and its application has been very successful in describing three-body dynamics in a continuum [7]. In the study of CSM, the tempered Gaussian basis is employed to obtain the continuum solutions. Thus, CSM plus the tempered Gaussian is considered to be an appropriate combination for the pragmatic calculation of the continuum resonances. In contrast to CSM, the so-called difference method [22,23], in which radial coordinates are discretized in a finite mesh, is mainly employed in the ABC calculation for nuclear systems [22]. For example, a three-body nuclear reaction, induced by the deuteron breakup,

is nicely described by the difference method plus ABC [22]. However, in nuclear systems, the application of Gaussian expansion methods to ABC is still limited to only a few examples of two- or three-body problems [20,21,24]. Many applications of ABC plus basis expansion exist in molecular physics [15–19], but the eigenfunction of the harmonic oscillator or Legendre polynomial has mainly been used as the basis function. In view of these situations, the authors think that the investigation of the applicability of the Gaussian basis to the ABC problem is interesting and instructive.

In the present paper, we focus on several types of Gaussian basis functions, which are standard in basis expansion methods, and their applicability to ABC is explored in a schematic two-body problem. There are two versions of the tempered Gaussian basis: the shifted Gaussian [5] and the oscillating Gaussian [3,4]. The shifted Gaussian is generated by shifting the peak position of the tempered Gaussian to a finite distance S, such as $e^{-\nu(r-S)^2}$. A set of the shifted Gaussian is obtained by varying the center position of S according to the arithmetic progression. The oscillating Gaussian, which has been recently proposed, is given by a product of the tempered Gaussian and the trigonometric function such as $\sin(\nu r^2)e^{-\nu r^2}$ and $\cos(\nu r^2)e^{-\nu r^2}$. Both the shifted and oscillating Gaussian are appropriate for describing highly oscillating functions, in which the wave function has a large number of radial nodes. In the ABC calculation, continuum wave functions reveal highly oscillating behavior at a large distant region. Therefore, the shifted and oscillating Gaussians are expected to be feasible in the ABC problem. We employ the three kinds of basis, the tempered, shifted, and oscillating Gaussians in the ABC calculation, and the basis dependence of the continuum solutions will be reported in detail.

The organization of this article is as follows: In Sect. 2, the employed Hamiltonian and the basis functions are briefly explained. In Sect. 3, the energy distributions of the eigenvalues obtained by the different Gaussian basis are investigated in the complex energy plane. We also discuss the behavior of the wave functions in the resonant and continuum states. In the last part of Sect. 3, the sensitivity of the resonant states with respect to the variation of the strength of the absorbing potential is analyzed. In this analysis, the optimization of the resonance parameters and the resonance trajectory in the complex energy plane are discussed. The final section is devoted to the discussion and summary.

2. Framework

2.1. *Model Hamiltonian with an absorber*

In the present analysis, we employ a model Hamiltonian with a schematic potential [25] as follows:

$$H = -\frac{\hbar^2}{2m}\nabla^2 + V(r), \tag{1}$$

$$V(r) = -V_1 e^{-\mu_1 r^2} + V_2 e^{-\mu_2 r^2}. \tag{2}$$

Here the parameters of the potential $V(r)$ are chosen as $V_{1,2} = 8.0$ (MeV), 4.0 (MeV) and $\mu_{1,2} = 0.16$ (fm^{-2}), 0.04 (fm^{-2}). In this Gaussian potential, there are short-range attractive and long-range repulsive parts. The former attractive part corresponds to the nuclear interaction, while the latter repulsive part simulates a Coulomb barrier. In the kinetic energy part, we set $\frac{\hbar^2}{m}$ (MeV·fm^2) $= 1$ for simplicity. Thus, the dimension of the energy equals the (length)$^{-2}$. The complex scaling method (CSM) was applied to the resonance problem in this potential, and the resonant energies are reported in Ref. [11].

In solving the eigenvalue problem for the Hamiltonian in Eq. (1) under the absorbing boundary condition (ABC), we simply add the negative imaginary potential $-iW(r)$ with a strength η, such as

$$H^\eta = H - i\eta W(r), \tag{3}$$

and the Schrödinger equation for H^η is solved by the basis expansion method. We should choose the functional form of the absorber $W(r)$. The functional form of $W(r)$ is not arbitrary and various conditions are required as discussed in Ref. [15].

The important requirement of an absorber $W(r)$ is given by

$$\Re[W(r)] \geq 0, \quad r \geq 0$$
$$\Re[W(r)] \to \infty, \quad r \to \infty. \tag{4}$$

Furthermore, the absorber should be polynomially bound to obtain the correct convergence of the resonance wave function at an asymptotic region. Therefore, the exponential potential $W(r) = \exp(\alpha r)$ cannot be used as an absorber. Although there is a theoretical development in the absorbing potential [26], we employ the shifted polynomial function such as

$$W(r) = \theta(r - r_a) \cdot (r - r_a)^p. \tag{5}$$

The polynomial absorber is standard and has been usually employed in previous studies [15–24]. A starting point of the absorber r_a should be taken to the outside of the physical interaction region. The power of the polynomial is set to $p = 4$ in the present calculation. According to the analysis in Ref. [20], the lower power, such as $p = 2$, has been proven to be appropriate for searching a broad resonance existing around zero energy. However, in the absorber with the lower power, the minimization of the error, contained in the resonance parameter (resonance energy and the decay width), is somewhat difficult. The power of $p = 4$ has been found to reduce the errors in the resonance parameter [20,24] and, hence, we use the power of $p = 4$ in the present calculation.

2.2. *Basis expansion method*

The total wave function $\Psi(\mathbf{r})$ is given by a product of the radial part $\chi_L(r)$ and the spherical harmonics $Y_{LM}(\hat{\mathbf{r}})$ with the orbital angular momentum L and its third component M. According to a standard technique in a variational calculation, the radial part of the wave function $\chi_L(r)$ is expanded by a series of the basis functions $u_{mL}(r)$, such as

$$\Psi(\mathbf{r}) = \chi_L(r) \cdot Y_{LM}(\hat{\mathbf{r}}) = \sum_{m=1}^{M} C_{mL} \frac{u_{mL}(r)}{r} \cdot Y_{LM}(\hat{\mathbf{r}}), \tag{6}$$

and we solve a set of the generalized eigenvalue equation for the mixing amplitude of C_{mL} and the energy eigenvalue E

$$\sum_{m=1}^{N} \left(H_{nm}^{(L)\eta} - E N_{nm}^{(L)} \right) C_{mL} = 0 \ (n = 1 \sim M) \tag{7}$$

with the matrix elements of $H_{nm}^{(L)\eta} = \langle u_{nL}|H^{(L)\eta}|u_{mL}\rangle$ and $N_{nm}^{(L)} = \langle u_{nL}|1|u_{mL}\rangle$. The energy eigenvalue E is a complex number, which has the relation of $E = E_R - i\Gamma_R/2$ with the resonance energy E_R and the resonance width Γ_R. Here $H^{(L)\eta}$ represents the Hamiltonian for the partial wave L,

$$H^{(L)\eta} = H^{(L)} - i\eta W(r) \tag{8}$$

$$H^{(L)} = -\frac{1}{2}\frac{d^2}{dr^2} + \frac{L(L+1)}{2r^2} + V(r). \tag{9}$$

In the present calculation, we handle the $L = 1$ problem, which has the same conditions as the CSM study in Ref. [11].

According to Eq. (8), the Hamiltonian matrix $H^{(L)\eta}_{nm}$ can be simply decomposed into two parts:

$$H^{(L)\eta}_{nm} = H^{(L)}_{nm} - i\eta W_{nm} \tag{10}$$

with $W_{nm} = \langle u_{nL}|W|u_{mL}\rangle$. Equation (10) means that any computational programs for the bound-state problem, in which the matrix elements of $H^{(L)}_{nm}$ are calculated, can be directly used in the method of ABC. That is, we can introduce the absorbing boundary condition by just adding the matrix elements of the absorber, $-i\eta W_{nm}$, to the matrix elements of the original Hamiltonian, $H^{(L)}_{nm}$. This is one of the advantages in the absorbing boundary condition. In a pragmatic ABC calculation, however, we must superpose many basis functions over a wide spatial range. The necessity of the wide superposition is because the reflection effect, which arises from the existence of the absorber, should be minimized as much as possible.

2.3. *Types of Gaussian basis*

In the variational calculation under the absorbing boundary condition, we use three kinds of Gaussian functions for the basis of $u_{nL}(r)$: (1) a shifted Gaussian (SG), (2) a tempered Gaussian (TG), and (3) an oscillating Gaussian (OG). In the following, we briefly explain the individual Gaussian bases.

(1) Shifted Gaussian basis. The functional form of the shifted Gaussian (SG) basis is

$$u_{nL}(r) = N_n r e^{-\nu(r-S_n)^2} \tag{11}$$

$$S_n = S_1 + (n-1)\Delta S. \tag{12}$$

Here N_n represents the normalization constant. S_n is a variational parameter generated by an arithmetic progression in Eq. (12) with a constant difference ΔS, and it approximately gives a peak position of the nth basis function. The parameter S_n is often called the "distance parameter". Usually, the width parameter ν is taken to be a common value. A superposition of the SG basis is possible to construct a highly oscillating function. Thus, the SG basis can handle highly excited states, in which the higher nodal excitation occurs in the wave function. In the calculation of the matrix elements, however, we must rely on the numerical integration, and numerical precision should be carefully checked in an integration.

The SG function is one of the standard basis functions of the microscopic cluster model in the framework of the generator coordinate method (GCM) [5,20]. In GCM, the basis function is called the locally peaked Gaussian, which is given by the product of the modified spherical Bessel function and the tempered Gaussian. The shifted Gaussian in Eq. (11) corresponds to the asymptotic form of the locally peaked Gaussian, which is obtained by taking the limit of S_n or $\nu \to$ large. In the locally peaked Gaussian, there is the L dependence, but, on the basis of Eq. (11), the L dependence of the basis functions vanishes. Thus, the SG basis itself does not satisfy the asymptotics of $u_{nL}(r \to 0) \sim r^{L+1}$. The asymptotics of the wave function at $r \to 0$ is possible to achieve in the superposition of the SG basis under the variational principle.

(2) Tempered Gaussian basis. The tempered Gaussian (TG) basis is a series of the Gaussian function obtained by varying the width parameters. The explicit functional form of the nth basis with L is given by

$$u_{nL}(r) = N_{nL} r^{L+1} \exp\left(-\nu_n r^2\right), \tag{13}$$

$$\nu_n = \frac{1}{2b_n^2}, \quad b_n = b_1 a^{n-1}. \tag{14}$$

Here N_{nL} is a normalization constant for the nth TG basis. The width parameters b_n are generated according to a geometric progression with the constant geometric ratio a. The TG basis has a smooth radial dependence and, hence, it is appropriate to construct slowly oscillating functions, which mainly appear in a ground state or low-lying states.

The TG basis has been widely used especially in few-body calculations because the matrix elements can be calculated in an analytic manner if the interaction is expressed in terms of the polynomial, Gaussian, and exponential functions on r [1]. Thus, mathematical treatments of the matrix elements are easy in numerical calculations. Furthermore, the TG basis is good in describing weakly bound systems, in which a tail of the wave function slowly damps beyond the classical turning point. This applicability of the TG basis is because the superposition of the TG basis can reproduce the exponentially damping function, which appears outside of a classical turning point.

(3) Oscillating Gaussian basis. The TG basis in Eq. (13) has a smooth radial dependence, but an oscillating feature can be implemented by a complex scaling on the width parameter, $\nu_n \to (\alpha + i\beta)\nu_n$. The scaled function $\phi_{nL}(r)$ becomes

$$\phi_{nL}(r) = r^{L+1} \exp\left(-(\alpha + i\beta)\,\nu_n r^2\right). \tag{15}$$

A series of the oscillating Gaussian basis (OG) is generated from the linear combination of $\phi_{nL}(r)$ and $\phi^*_{nL}(r)$,

$$u_{nL}(r) = N_{nL}\left(\phi^{\cos}_{nL}(r) + \phi^{\sin}_{nL}(r)\right), \tag{16}$$

$$\begin{aligned}\phi^{\cos}_{nL}(r) &= \tfrac{1}{2}\left[\phi_{nL}(r) + \phi^*_{nL}(r)\right] \\ &= r^{L+1}\exp\left(-\alpha\nu_n r^2\right)\cos\left(\beta\nu_n r^2\right),\end{aligned} \tag{17}$$

$$\begin{aligned}\phi^{\sin}_{nL}(r) &= \frac{i}{2}\left[\phi_{nL}(r) - \phi^*_{nL}(r)\right] \\ &= r^{L+1}\exp\left(-\alpha\nu_n r^2\right)\sin\left(\beta\nu_n r^2\right).\end{aligned} \tag{18}$$

Here N_{nL} represents the normalization constant of the total basis function. The scaling parameters α and β are usually fixed to a certain value in solving the eigenvalue problem of the total Hamiltonian. The width parameters ν_n are generated by the geometrical progression shown in Eq. (14). $\phi^{\cos}_{nL}(r)$ and $\phi^{\sin}_{nL}(r)$ are the product of the TG basis and the trigonometric functions, and the smoothed radial behavior in the TG basis and the oscillating feature in the trigonometric functions are combined in the OG basis. Due to this combination, the OG basis is considered to describe both the smooth and oscillating functions. Therefore, the OG basis can handle highly excited states as well as less excited states in a consistent manner. In addition, the mathematical structure of the OG basis is basically the same as that of the TG basis and, hence, the matrix elements of the OG basis can be evaluated in an analytical way similar to the TG basis.

2.4. *Details of the computational conditions*

The matrix elements of the original Hamiltonian $H^{(L)}_{nm}$ are analytically evaluated for the TG and OG bases, while the numerical integration is performed for the SG basis. The starting point of the shifted absorbing potential in Eq. (5) is set to $r_a = 7$ fm. In the evaluation of the matrix elements of the shifted absorber, W_{nm}, we must employ the numerical integration for all the basis functions. All the numerical integration is done on the basis of the Gauss–Legendre method. The radial integration is

Table 1. Set of the variational parameters. "min." and "max." denote the minimum and maximum values of the variational parameters for the SG, TG, and OG bases. The additional parameters (α, β) in the OG basis are $(\alpha, \beta) = (1,3)$, while ν and ΔS in the SG basis are $\nu = 2$ fm^{-2} and $\Delta S = 0.5$ fm, respectively. $\sqrt{r^2}_{\max}$ represents the root-mean-squared radius of the maximum basis functions. All the lengths are shown in units of fm.

Basis	prm.	min.	max.	N	$\sqrt{\langle r^2\rangle}_{\max}$
SG	S_n	0.10	29.6	60	29.6
TG	b_n	3.0×10^{-4}	40.0	100	63.2
OG(cos)	b_n	1.00	15.0	30	24.3
OG(sin)	b_n	1.00	15.0	30	23.1

performed up to about 80 fm for the SG and OG bases and 200 fm for the TG basis. A whole spatial region is decomposed into bins of 1.2 fm, and twenty-four mesh points are prepared for each of the spatial bins. We have checked the numerical precision of the integration by changing the size of the bin. The integration value of the matrix elements of the absorber W_{nm}, for instance, is converged in the order of magnitude of $\sim 10^{-8}$.

A set of the variational parameters for the individual Gaussian basis functions is listed in Table 1. There are two parameter sets for the OG basis, the sine and cosine types. In the present calculation, both the basis functions are included according to Eq. (16). In this table, the minimum (min.) and maximum (max.) values of the variational parameters are shown. The root-mean-squared radius of the maximum basis ($\sqrt{\langle r^2\rangle}_{\max}$ in the rightmost column) represents the maximum distance that can be covered by each of the basis functions. In the calculation of the absorbing boundary condition, a series of the basis functions should cover the spatial region outside of the interaction range in order to describe the smooth damping of the continuum wave function. However, an instability appears in solving the generalized eigenvalue equation (7) if we extend the range of the basis function and the starting point of the absorber r_a to a much larger distance. For example, in the unstable solutions, a series of the continuum states, which will be explained in the following section, is not in a regular sequence, but in a random distribution in the complex energy plane. Thus, there is an optimal size in the maximum range of the basis function in the pragmatic calculation. In the present calculation, we set the computational range to be the region of $r \leq 30$ fm. The sequence of the continuum energy levels and the errors contained in the resonance parameters are optimized as much as possible within this spatial range. We have confirmed that the computational results are not drastically improved even if the spatial range of the basis functions is extended to a larger distance than $r \sim 30$ fm.

The $\sqrt{\langle r^2\rangle}_{\max}$ value of the OG basis is the smallest (23.1 fm for the sine OG), while that of the TG basis is the largest (63.2 fm) of all the basis functions. The maximum range of the TG basis is much larger than the previous study in Ref. [24]. The long-range setting of the TG basis is due to the generation of the orthogonal basis set. The SG, TG, and OG bases are non-orthogonal functions and, hence, the orthogonal basis must be constructed in solving Eq. (7). The orthogonal bases are generated by diagonalizing the norm matrix $N^{(L)}_{nm}$, and then the Hamiltonian matrices $H^{(L)\eta}_{nm}$ are reconstructed by the orthogonalized basis. In generating the orthogonal basis, we must set a minimum eigenvalue $\lambda_{\min}$ for the diagonalization of the norm matrix and exclude the orthogonal basis that has an eigenvalue smaller than $\lambda_{\min}$. This exclusion is because an orthogonalized basis belonging to an extremely small norm eigenvalue induces a numerical instability. Thus, the original number of the non-orthogonal basis (N in Table 1) is reduced to the "effective number" of orthogonalized basis.

In Table 2, the lower limits of the norm eigenvalue ($\lambda_{\min}$) are listed in the second column from the

Table 2. The lower limit of the norm eigenvalues, $\lambda_{\min}$, that accepts the orthogonalized basis. In the third column from the right, the number of excluded orthogonalized bases is shown. The percentage (%) of the accepted basis number to the total basis number are shown in the following column. The $\sqrt{\langle r^2\rangle}_{\max}$ of the orthogonalized bases are shown in the rightmost column (units in fm). All the results are obtained for the variational parameter sets shown in Table 1.

Basis	$\lambda_{\min}$	Excluded	Accepted (%)	$\sqrt{\langle r^2\rangle}_{\max}$
SG	10^{-7}	0	100	17.8
TG	10^{-7}	40	60	36.8
OG	10^{-7}	0	100	25.1

left. For individual bases, $\lambda_{\min}$ is fixed so as to reproduce the regular sequence of the energy eigenvalues and optimize the resonance parameters as much as possible. In the SG and OG calculations, all the orthogonal bases are accepted and, hence, the effective basis number is 60, which is the same as the number shown in Table 1 ($N = 60$). However, the accepted percentage of the orthogonalized basis is about 60% in the TG basis under the condition of $\sqrt{\langle r^2\rangle}_{\max} = 63.2$ fm. Thus, the effective number is reduced to 60 from the original number of $N = 100$. If the value of $\sqrt{\langle r^2\rangle}_{\max}$ in the TG basis is restricted to be $\sqrt{\langle r^2\rangle}_{\max} \leq 30$ fm, generation of the 60 orthogonalized TG bases, which is the same effective number as the SG and OG basis functions, is difficult. To keep the effective number of the orthogonalized basis common between the SG, TG, and OG bases, the maximum range of the TG basis must be exceptionally extended to be $\sqrt{\langle r^2\rangle}_{\max} = 63.2$ fm, as shown in Table 1. Since the non-orthogonality of the TG basis is the most prominent of all the basis functions, the spatial range of the TG basis must be extended to generate a series of the orthogonalized TG basis, which is comparable to the orthogonalized SG and OG bases.

In the rightmost column of Table 2, the mean radii for the orthogonalized bases are listed. The radii of the orthogonalized SG and TG bases are 17.8 fm and 36.8 fm, respectively, which are reduced to half in comparison to the respective radii before orthogonalization, shown in Table 1 (29.6 fm for SG and 63.2 fm for TG). The SG and TG bases have a nodeless distribution, and one peak exists at an external region. If the orthogonalization is imposed on such smooth bases, a finite amplitude with an oscillation appears in the inner region. The appearance of the inner oscillation leads to the reduction of the radius of the SG and TG bases. In contrast, the radius of the OG basis is almost invariant under the orthogonalization; the orthogonalized radius is 25.1 fm, while the non-orthogonal radius is about 24 fm (Table 1). In contrast to the SG and TG bases, an inner oscillation is originally implemented in the OG basis by introducing the trigonometric function. Thus, an orthogonalization is not so effective on the OG basis. This is the reason why the radius of the OG basis is almost invariant under the orthogonalization.

2.5. Schematic picture of the eigenvalues

The eigenvalues calculated from the Hamiltonian with an appropriate absorber that satisfies the conditions in Ref. [15] becomes a purely discrete spectrum for all $\eta > 0$. Figure 1 shows a schematic picture of the energy spectrum in the complex energy plane when the polynomial function shown in Eq. (5) is employed as an absorbing potential. The energy sequence shown in Fig. 1 is empirically established through the numerical calculations with the harmonic oscillator basis [15–17]. In this figure, the angle θ is given by the relation of $\theta = -\pi/(2 + p)$ with the power of the absorber

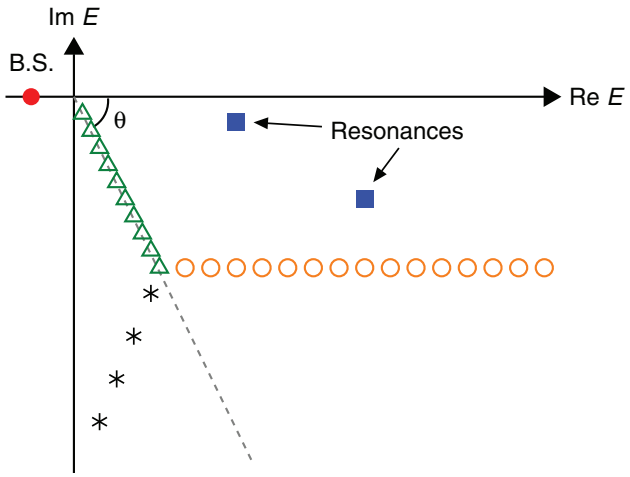

Fig. 1. Schematic picture of the eigenvalues calculated from the Hamiltonian with a polynomial absorber. Eigenvalues are plotted in a complex energy plane. See text for details.

p [15,20]. One can clearly distinguish four groups of eigenvalues shown by the various symbols. The individual symbols have the following meanings:

(1) Isolated states (solid symbols). The bound states (solid circle, B.S.) should be invariant under the addition of the absorber. The resonant states are shown by solid squares, which are surrounded by the line with a rotation angle θ, the real axis, and the string of eigenvalues parallel to the real axis.

(2) Converged non-resonant states (open triangles). A series of eigenvalues appears along the θ axis. The wave function in these eigenvalues is smoothly damped within the computational radial space due to the effect of the absorber.

(3) Indifferent states (open circles). In the levels parallel to the real axis, the wave functions strongly oscillate, and they are almost real. Due to their comparatively high real energy, these states are only weakly affected by the absorber and they are reflected at the end of the spatial grid.

(4) Diverging states (asterisks). A few eigenvalues exist below the θ axis. The wave functions for the diverging state have a large amplitude at a large distance region. These non-converging states are an artifact of the incomplete finite basis set.

3. Results

3.1. Energy distributions

In this section, we compare the distribution of the energy eigenvalues obtained for the three different Gaussians, the SG, TG, and OG bases. In Fig. 2, the energy eigenvalues for the $L = 1$ states are plotted in the complex energy plane. Panels (a), (b), and (c) show the results of the SG, TG, and OG bases, respectively.

The strength of $\eta = 1.8 \times 10^{-5}$ is used for the SG calculation, and the result is shown in Fig. 2(a). In this figure, there are three isolated levels shown by the double squares. The negative energy state around $\Re[E] = E_R \sim -0.7$ fm^{-2} is a bound state, while the positive energy state around $E_R \sim 1.17$ fm^{-2} is the first resonant state. The width of this resonance is quite small ($\Gamma_R/E_R \sim 10^{-2}$) and hence it appears quite close to the real axis. The second resonance appears at $E_R \sim 2$ fm^{-2} and $\Gamma_R/2 \sim 0.5$ fm^{-2} with a broad width ($\Gamma_R/E_R \sim 0.5$). These two resonances are clearly separated

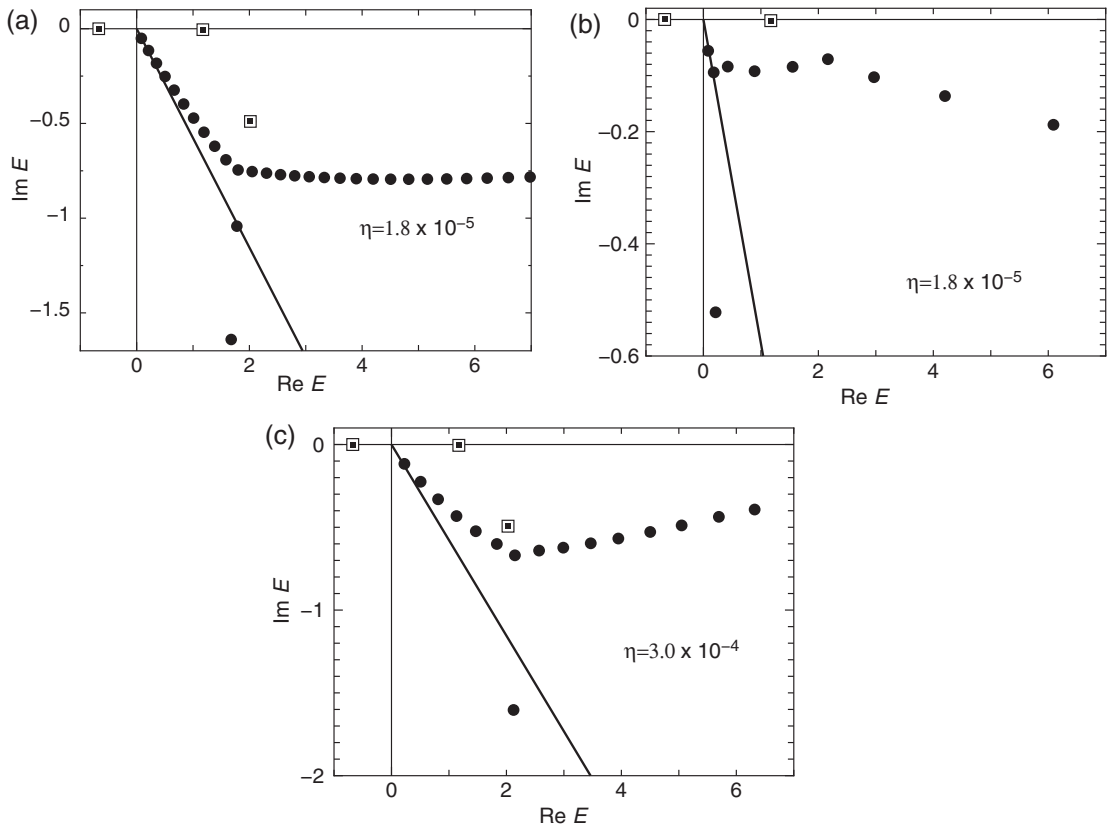

Fig. 2. Energy eigenvalues plotted in the complex energy plane. The abscissa and ordinate represent the real and imaginary parts of the eigenvalues, respectively. Panel (a) shows the result of the SG basis, while the results of the TG and OG bases are plotted in panels (b) and (c), respectively. The line plotted from the origin denotes the rotation angle for the converged state ($\theta = -\pi/6$). In all of the panels, the isolated states are shown by double squares, while the continuum states are plotted by solid circles.

from the continuum states (solid circles) because the imaginary part of the continuum states is systematically larger than that of the separated resonant states. In the continuum states, we confirm a regular sequence, which splits into three lines. Since the power of $p = 4$ is employed for the absorber, the converged continuum states are on the $\theta = -\pi/6$ axis (solid line), although they slightly deviate from the θ axis in the higher energy region. The series of continuum levels parallel to the real axis belongs to the line of the indifferent continuum states, while the two continuum levels appearing below the θ axis correspond to the diverging states.

In contrast, we can see strange behavior in the energy distribution for the TG solutions (Fig. 2(b)). Here the strength of the absorber is set to be $\eta = 1.8 \times 10^{-5}$. The bound and first resonant states (double squares) can be clearly identified, but the regular structure of the splitting straight lines is broken. In addition, the level density solved by the TG basis is much lower than that solved by the SG basis. All the continuum states have a small imaginary part, and they locate at the region close to the real axis. This result means that the solutions obtained by the TG basis do not feel the absorption much; nevertheless, the maximum range of the TG basis is a much larger value than the SG basis. The imaginary parts of the continuum energy levels are almost invariant even if the strength of the absorber is artificially increased. Thus, the continuum states calculated by the TG basis are quite insensitive to the variation of the strength of the absorber. Since the effect of the absorber is small

for the TG basis, the second resonance with a large imaginary part cannot be separated from the continuum states.

The variational calculation of the TG basis was also done for a similar Gaussian potential in Ref. [24]. In this calculation, the resonant state with a broad width ($\Gamma_R/E_R \sim 0.7$) was identified, although the setting of the computational condition in Ref. [24] was different from the present calculation. In the analysis of Ref. [24], the higher power of the radial coordinate is multiplied to the original TG basis in order to identify the broad resonance. Due to this modification, the TG basis can include the higher nodal property of the wave function. Therefore, to calculate the broad resonant states, not only a simple extension of the maximum range, but also the modification of the functional form will be needed for the TG basis.

The energy distribution calculated by the OG basis is shown in Fig. 2(c). In this calculation, two resonances (double squares at $\Re[E] > 0$) are clearly separated from the continuum line. Here we use the absorber strength of $\eta = 3.0 \times 10^{-4}$, which is stronger than the strength in the SG and TG calculations ($\eta = 1.8 \times 10^{-5}$). The second resonance located at $E_R \sim 2$ fm^{-2} is not separated from the continuum state if the strength of $\eta = 1.8 \times 10^{-5}$ is adopted. Thus, in the OG calculation, the strength of the absorber is increased to identify the second resonance.

The distribution of the continuum levels in the OG calculation is considerably different from the regular sequence observed in the SG calculation. A few continuum states starting from the origin follow the converged continuum line of $\theta = -\pi/6$ in the lower energy region, but the imaginary part of the continuum states gradually decreases as the real part of the eigenvalues becomes high. As a result of this decrease of the imaginary part, the series of the continuum states, corresponding to the indifferent states, is not parallel to the real axis in the higher energy region. The sequence of the continuum levels draws not a straight line, but a smooth curve, and the shape of the curve depends on the strength of the absorber. The level density of the OG basis is considerably higher than that of the TG basis, but the density is still lower than the result of the SG basis.

3.2. Wave functions in the continuum

The difference of the energy distributions, confirmed in Fig. 2, strongly suggests that the absorbing effect is noticeably different among the employed basis functions. In order to see the effect of the absorber more clearly, we analyze the wave functions for the continuum states. We show four kinds of wave functions according to the categories in Fig. 1: (1) isolated resonant state, (2) converged non-resonant states, (3) indifferent state, and (4) diverging state.

In the upper panel of Fig. 3, the continuum energies calculated from the SG basis are plotted, while the real part of the reduced wave functions, $r\chi_L(r)$ ($L = 1$), are shown in the lower four panels, (1)–(4). The wave functions shown in the lower panels of (1)–(4) correspond to the levels of (1)–(4) in the upper panel (double squares), respectively. The resonance wave function shown in panel (1) has a large amplitude inside of the interaction region, and the amplitude penetrates into the interaction-free region. The penetrating part strongly oscillates, and its amplitude is smoothly damped as the distance becomes larger. The smooth oscillation and damping is generated by the absorber, which starts at $r_a = 7$ fm.

In contrast, there is a difference in the distribution of the wave functions among the non-resonant continuum shown in Fig. 3, panels (2)–(4). In the converged non-resonant state in panel (2), the wave function is smoothly damped in the spatial region of $r \leq 30$ fm, which is covered by the basis states (see Table 1). There is a strong oscillation in the indifferent state (3), and its maximum amplitude is

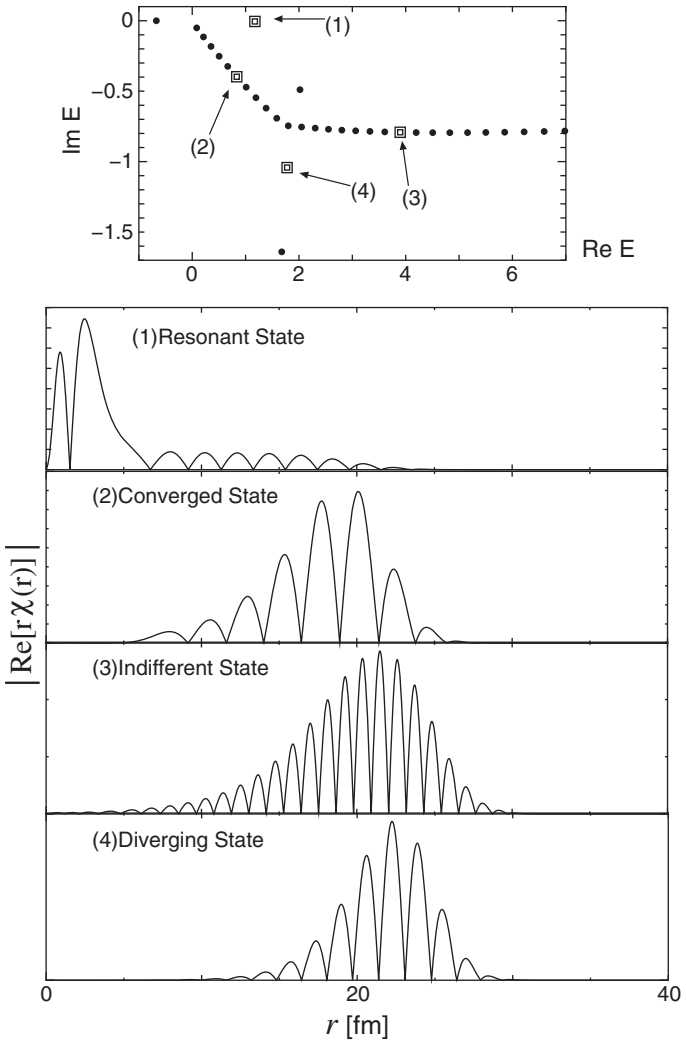

Fig. 3. Wave functions obtained for the SG basis. In the top panel, the energy levels in the complex plane are shown, and are the same as in the panel (a) in Fig. 2. In panel (1), the wave function of the resonant state is shown, while the converged non-resonant wave function is plotted in panel (2). Panels (3) and (4) show the wave functions for the indifferent and diverging states, respectively. The ordinate in panels (1)–(4) show the amplitude of the real part of the wave function, plotted in arbitrary units.

shifted to the outer region in comparison to the converged state (2). The distribution of the diverging state (4) is localized at the largest distance region of all the continuum states. The amplitudes of (3) and (4) are rapidly damped around the end point of the maximum basis, $S_{\max} = 30$ fm. This rapid damping means that both the indifferent state (3) and the diverging state (4) are generated by the incompleteness of the finite basis expansion. All the non-resonant continuum wave functions extensively oscillate at the interaction-free region. To get a regular sequence of the energy eigenvalues in the complex plane, therefore, a superposition of the basis functions should describe the extensive oscillation of the wave function over a wide distance region.

The same analysis on the wave functions is shown in Fig. 4 for the TG basis. In the upper panel, we select the four continuum states (double squares) that have almost the same complex energy as the four levels shown in the upper panel of Fig. 3. The respective wave functions are plotted in the lower four panels, Fig. 4, panels (1)–(4). The shape of the resonant wave function in Fig. 4, panel (1) is

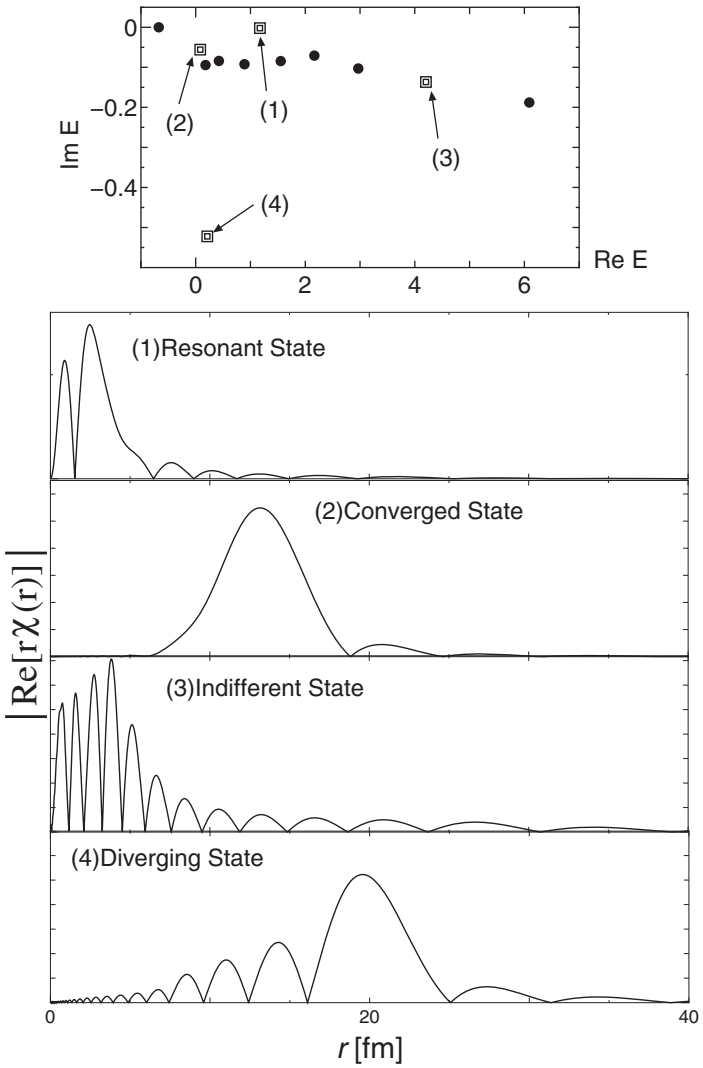

Fig. 4. The same as Fig. 3, but for the results obtained by the TG basis.

almost the same as the SG resonance in Fig. 3, panel (1), although the oscillation of the TG resonance around $r \geq 5$ fm is weaker than the SG resonance. We can confirm that the oscillating pattern of the non-resonant wave functions, Fig. 4, panels (2)–(4), in the TG basis is noticeably different from the wave function in the SG basis, shown in Fig. 3, panels (2)–(4).

The peak position of the converged continuum solution in Fig. 4, panel (2) is shifted to a shorter distance than that of the SG converged state, shown in Fig. 3, panel (2), and the oscillation of the TG solution is much weaker than that of the SG solution. The indifferent state in Fig. 4, panel (3) has a strong oscillation, but its main amplitude is noticeably concentrated on the interaction region, about $r \leq 5$ fm. This distribution in the TG solution is very different from the respective SG solution in Fig. 3, panel (3), in which the maximum amplitude appears at the larger distance region. The diverging state in Fig. 4, panel (4) also reveals the weak oscillation behavior in comparison to the respective SG solution in Fig. 3, panel (4).

The continuum levels and the respective wave functions calculated by the OG basis are shown in the upper panel and the lower four panels ((1)–(4)) in Fig. 5, respectively. The oscillation of the OG resonant state in Fig. 5, panel (1) is similar to the respective SG resonance in Fig. 3, panel (1), but the

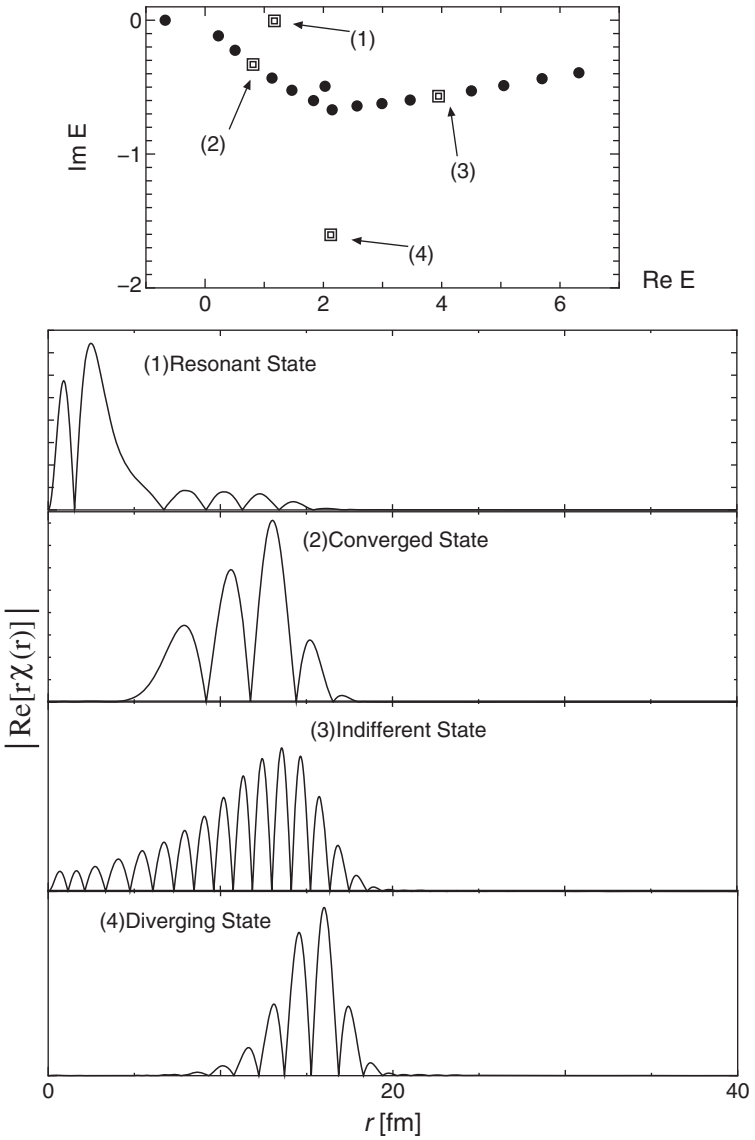

Fig. 5. The same as Fig. 3 but for the results obtained by the OG basis.

damping of the OG resonance rapidly occurs. The nodal behaviors of the non-resonant continuum in Fig. 5, panels (2)–(4) is almost the same as that of the SG continuum states in Fig. 3, panels (2)–(4). However, the distributions of all the non-resonant wave functions in Fig. 5, panels (2)–(4) are shifted to the shorter distance region in comparison to the SG non-resonances, shown in Fig. 3, panels (2)–(4).

One of the possible reasons why the shrinkage of the wave functions occurs in the OG calculation is because the strength of the absorber is increased in the OG calculation ($\eta = 3.0 \times 10^{-4}$). The wave function is checked by performing the OG calculation with the weak strength of $\eta = 1.8 \times 10^{-5}$, which is the same strength as the SG calculation. In this calculation, we have found that the amplitude of the OG wave function tends to concentrate around a shorter radial region than that of the SG wave function. The other possible reason for the shrinkage is the small radius of the employed OG basis (see Table 1). To check the sensitivity to the maximum radius of the OG basis, we have done an extended calculation, in which the maximum radius of the basis state is increased to be $\sqrt{\langle r^2 \rangle}_{\max} \sim 30$ fm.

However, the distribution of the wave function is almost the same as the results shown in Fig. 5. Moreover, in such an extended calculation, the optimization of the resonance parameters, which will be explained in the next section, becomes worse.

The higher nodal behavior observed in the OG solutions is generated from the trigonometric functions multiplied by the tempered Gaussian, as shown in Eqs. (17) and (18) [1]. The distribution range of the OG continuum states is localized to the inner region in comparison to the SG continuum, and such a tendency can be seen especially in the indifferent state (3). This result means that the OG basis is feasible for describing the higher nodal states mainly appearing around the interaction region, while the SG basis can describe the extensive oscillation over a wide spatial region.

3.3. *Optimization of the resonance parameter*

In the previous section, we fixed the strength of the absorber, η, to a constant value. However, we search for an optimum value of η to determine the resonance energy and width. We denote the energy eigenvalue as a function of the parameter η, $E(\eta)$. If the basis set is complete, the correct resonance parameters can be obtained as a limit of $\eta \to 0$. In the finite basis set calculations, however, a finite η gives approximate resonance parameters. The condition for an optimal strength $\eta_{\rm o}$ is

$$\left| \eta \frac{dE(\eta)}{d\eta} \right|_{\eta=\eta_{\rm o}} = \text{min.} \tag{19}$$

Here the derivatives $\eta \cdot dE(\eta)/d\eta$ are obtained simply by employing the generalized Hellmann–Feynman theorem [27] like

$$\left| \eta \frac{dE(\eta)}{d\eta} \right| = \eta \left| \langle \tilde{\chi}_L^\eta | W | \chi_L^\eta \rangle \right| \equiv \langle W(\eta) \rangle, \tag{20}$$

where χ_L^η represents the relative wave function in Eq. (6) calculated with an absorber of the strength η. The tilde in the bra-state means that the complex conjugate is not taken in the radial integration.

An argument to justify the condition of Eq. (19) was presented on the basis of the asymptotic expansion of the function $E(\eta)$ [15,24]. Let us discuss the optimization of η in a simple argument. If η is very small and the range of the basis function is limited to the shorter region, absorption occurs in the region of large distance, where no basis functions exist. Then the resonant eigenvalue becomes almost real. As η increases, the absorption can be efficiently described by a given basis set, and the imaginary part of $E(\eta)$ increases. When the spatial region of the dominant absorption sufficiently overlaps the region of the basis functions, the imaginary part of $E(\eta)$ will be close to the true width. If one further increases η, the reflection due to the absorbing potential becomes substantial, and this will cause the imaginary part of $E(\eta)$ to decrease. Therefore, this consideration supports the conclusion that there is an optimal value of $\eta_{\rm o}$. The magnitude of the imaginary part in the eigenvalue exhibits stationary behavior around $\eta = \eta_{\rm o}$, which satisfies Eq. (19).

The η dependence of $\langle W(\eta) \rangle$ for the three bases, the SG, TG, and OG bases, is shown in Figs. 6, 7, and 8, respectively. Here the mesh of the strength is commonly taken to be $\Delta\eta = 1.0 \times 10^{-6}$. In all the figures, $\langle W(\eta) \rangle$ for the first resonance appearing around $E \sim 1.17$ fm^{-2} is plotted. In the result for the SG basis (Fig. 6), a minimum of $\langle W(\eta) \rangle$ appears at an optimal strength, $\eta_{\rm o}^{\rm SG} = 2.6 \times 10^{-5}$, and the minimum value of $\langle W(\eta) \rangle$ is 6.5×10^{-9} fm^{-2}. Around the optimal strength, a sharp minimum structure appears in $\langle W(\eta) \rangle$ of the SG solution.

The result of $\langle W(\eta) \rangle$ for the TG basis is shown in Fig. 7. The behavior of $\langle W(\eta) \rangle$ in the TG solutions is different from that in the SG solutions shown in Fig. 6. The minimum of the expectation value of

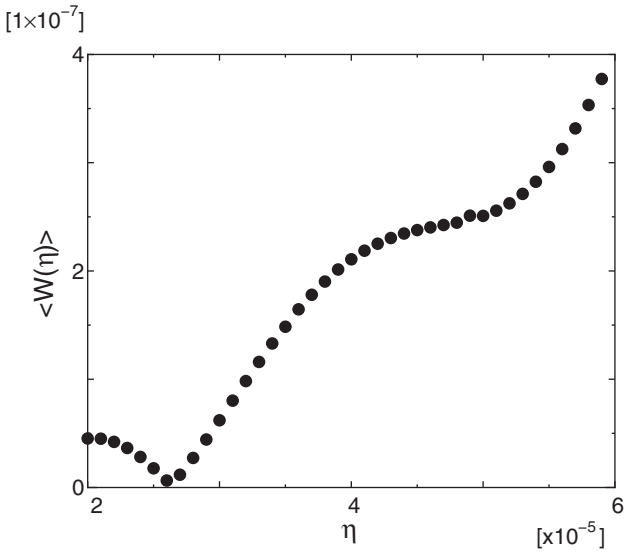

Fig. 6. η dependence of $\langle W(\eta)\rangle$ obtained for the SG basis. The abscissa and ordinate represent η and $\langle W(\eta)\rangle$, respectively. The scale of the abscissa (ordinate) should be multiplied by a factor of 10^{-5} (10^{-7}).

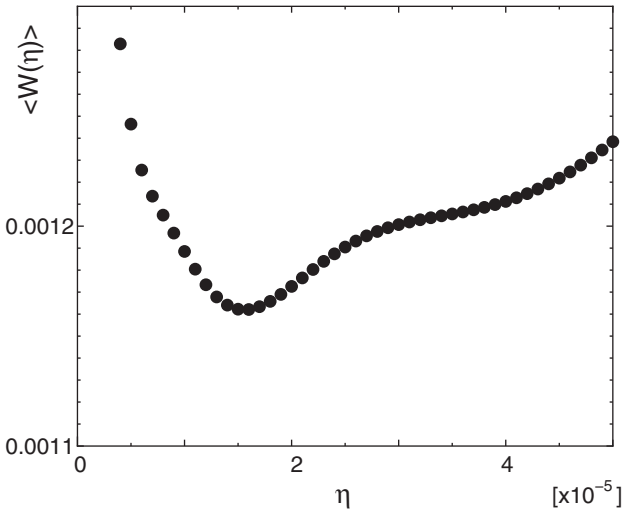

Fig. 7. Same as Fig. 6, but for the result calculated by the TG basis.

the absorber is $\langle W(\eta)\rangle = 1.2 \times 10^{-3}$ fm^{-2} at the optimal strength, $\eta_{\rm o}^{\rm TG} = 1.6 \times 10^{-5}$. In a series of $\langle W(\eta)\rangle$ for the TG solution, a broad minimum appears, and the $\langle W(\eta)\rangle$ varies smoothly around the optimal $\eta_{\rm o}^{\rm TG}$ value. In the OG basis shown in Fig. 8, the optimal strength is $\eta_{\rm o}^{\rm OG} = 3.0 \times 10^{-5}$, and the respective minimum value is $\langle W(\eta)\rangle = 7.2 \times 10^{-7}$ fm^{-2}. In the OG calculation, a sharp minimum structure appears in the curve of $\langle W(\eta)\rangle$, and the behavior of $\langle W(\eta)\rangle$ around the optimal $\eta_{\rm o}^{\rm OG}$ is similar to the result for the SG basis.

The resonance parameters (E_R and $\Gamma_R/2$) are determined at an optimal value of $\eta_{\rm o}$. The resonance parameters and $\langle W(\eta_{\rm o})\rangle$ at the optimal $\eta_{\rm o}$ are summarized in Table 3. The expectation value of $\langle W(\eta_{\rm o})\rangle$ represents a measure of errors in a resonance wave function at a given strength of $\eta_{\rm o}$, which arises from a finite set of the basis functions and a reflection from the absorber. The error of the SG solution is the smallest of all the basis calculations, while that of the OG solution is larger by two

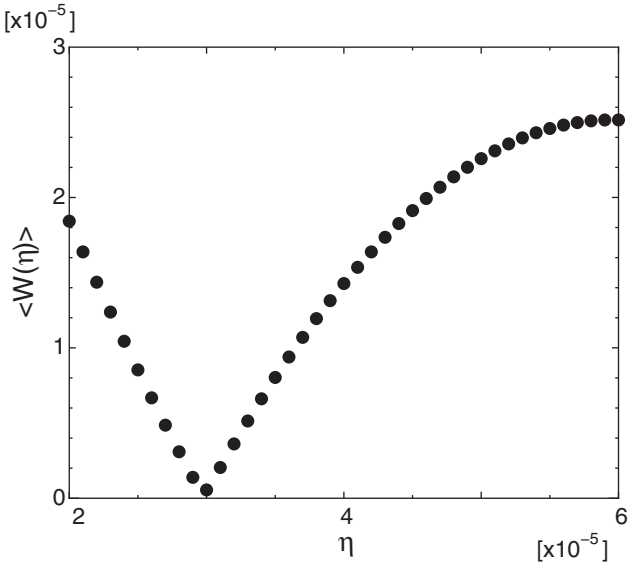

Fig. 8. Same as Fig. 6, but for the result calculated by the OG basis.

Table 3. Resonance parameters at an optimal strength of the absorber. E_R and Γ_R are the resonance energy and the decay width, respectively. η_o represents the optimal strength of the absorber, while $\langle W(\eta_o)\rangle$ shows the expectation value of the absorber, defined in Eq. (20), at an optimal η_o. In the bottom column, the resonance parameters calculated by the complex scaling method are shown for comparison. All the energies are plotted in units of fm^{-2}.

Basis	E_R	$\Gamma_R/2$	η_o	$\langle W(\eta_o)\rangle$
SG	1.174	4.97×10^{-3}	2.6×10^{-5}	6.5×10^{-9}
TG	1.172	2.03×10^{-3}	1.6×10^{-5}	1.2×10^{-3}
OG	1.172	4.91×10^{-3}	3.0×10^{-5}	7.2×10^{-7}
CSM [11]	1.171	4.86×10^{-3}	x	x

orders of magnitude. However, this result does not necessarily mean that the SG basis is superior because the magnitude of the error depends considerably on the precision of a whole numerical calculation. We really keep the precision of the numerical integration at about $\sim 10^{-8}$ in the matrix elements. This numerical precision corresponds to $\sim 10^{-13}$ for the matrix element of the absorber, $\eta_o W_{nm}$ in Eq. (10). However, there is a possibility that the minimum value of $\langle W(\eta_o)\rangle$ is changed by several factors, which depend on the numerical precision in solving the expansion coefficients, C_{mL}, in Eq. (7). Thus, in the present calculation, it is difficult to judge exactly whether the SG basis is superior to the OG basis or not, although both the SG and OG bases are considered to give at least better results than the result of the TG basis.

According to the difference in the error, $\langle W(\eta_o)\rangle$, the optimized resonance parameters are also different among these three bases. All the basis calculations give almost constant resonance energy, $E_R \sim 1.17$ fm^{-2}, but the decay width Γ_R in the TG solutions is smaller than in the other two bases. As shown in Fig. 3, panel (1), the tail part of the SG resonant wave function has an oscillation with a small amplitude. However, the TG resonant wave function in Fig. 4, panel (1) cannot completely follow the oscillation confirmed in the SG solution of Fig. 3, panel (1). This insufficient oscillating behavior of the tail part leads to a reduction of the decay width in the TG solution. The resonance parameter calculated from CSM is shown in the bottom row for comparison. The CSM calculation

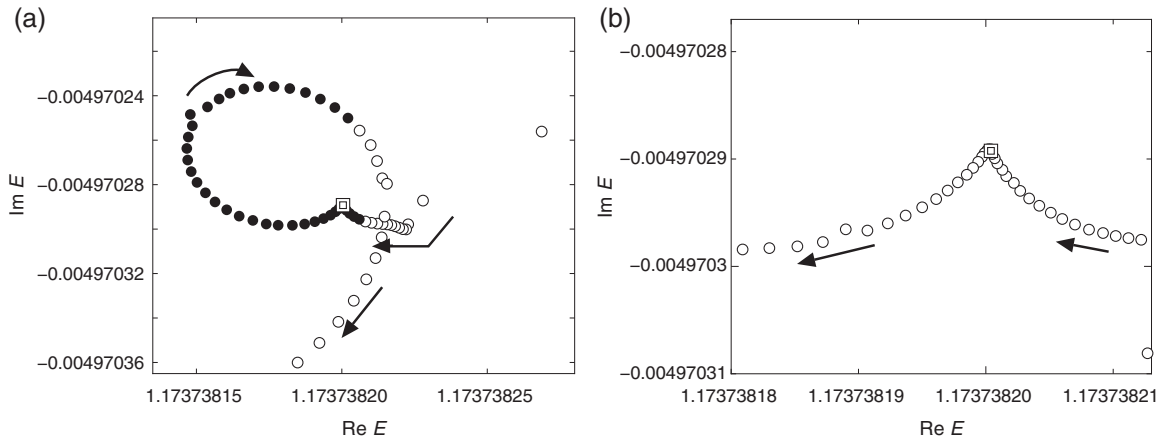

Fig. 9. η trajectory of the resonance eigenvalue in the complex energy plane. In panel (a), the double square shows the optimal point of the resonant level with $\eta = \eta_o^{SG}$. The solid circles show the eigenvalues around $\eta = \eta_o^{SG}$, and their variation range of η is the same as the abscissa in Fig. 6. Panel (b) is an enlargement of panel (a). In both panels, the abscissa and ordinate denote the real and imaginary parts of the eigenvalue, respectively. The arrows indicate the moving direction of the resonant state.

is performed by employing the harmonic oscillator basis function [11]. The SG and OG results are consistent with the result of CSM although the OG results seem to be close to the CSM calculation.

3.4. η trajectories of resonant states

We have confirmed that an optimal value of η really exists, which minimizes the error contained in the resonance parameter. In this section, we observe the η trajectory, which is the trajectory of the resonance eigenvalue generated by varying the strength of the absorber. In particular, we check the basis dependence of the η trajectory. According to the previous ABC studies in Refs. [15,18,19], the η trajectory of the resonance state reveals the stationary behavior around the optimal strength of η_o. Moreover, the CSM study [9,10] has pointed out that the stationary behavior (or "slow-down behavior" in the authors' terminology of Refs. [9,10]) occurs in the θ trajectory, which is a series of resonance eigenvalues obtained by varying the rotational angle θ. The resonance trajectory as a function of the controlling parameters, such as η in ABC or θ in CSM, is quite helpful in speculating on the position of the exact resonance eigenvalue in the case of an insufficient basis number.

Figure 9(a) shows the η trajectory of the SG basis. The mesh of the η trajectory is set to $\Delta\eta = 1.0 \times 10^{-6}$ for this calculation. In this trajectory, the resonant eigenvalue moves in a clockwise direction as the strength η increases, and the series of eigenvalues describes a circular trajectory. In this trajectory, the double square shows the eigenvalue at the optimal strength, $\eta = \eta_o^{SG}$, while the solid symbols denote the eigenvalues around the optimal strength. The variation range of η for the solid symbols in Fig. 9(a) is the same as the range of the abscissa shown in Fig. 6. Figure 9(b) is the enlargement of the η trajectory around $\eta = \eta_o^{SG}$ ($\Delta\eta = 5.0 \times 10^{-7}$). In Fig. 9(b), we can observe that a series of the eigenvalues becomes dense around the optimal strength of the absorber (double square). This dense behavior means that the resonant state is stationary with respect to the variation of the absorber strength; specifically, the resonance wave function is insensitive to the variation of the absorber strength just around $\eta = \eta_o^{SG}$. The circular trajectory in Fig. 9(a) and the stationary behavior in Fig. 9(b) are completely consistent with the previous analysis of ABC plus the harmonic oscillator basis [15,18,19].

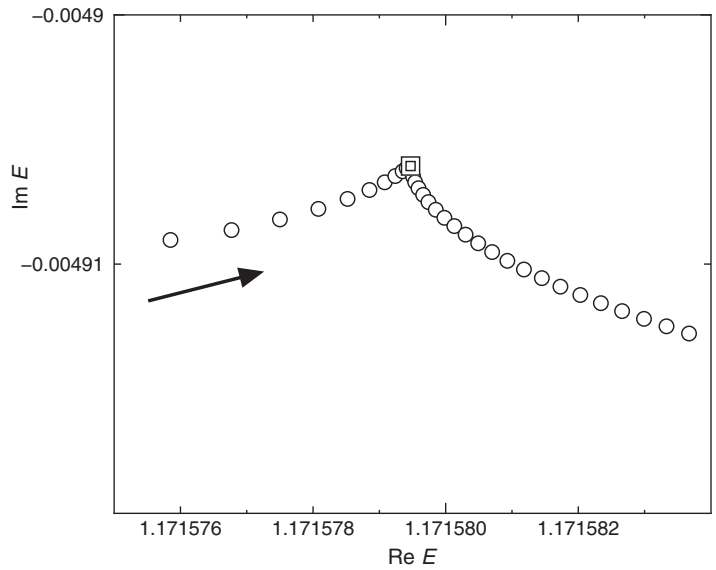

Fig. 10. Same as Fig. 9(b), but for the result calculated by the OG basis. See text for details.

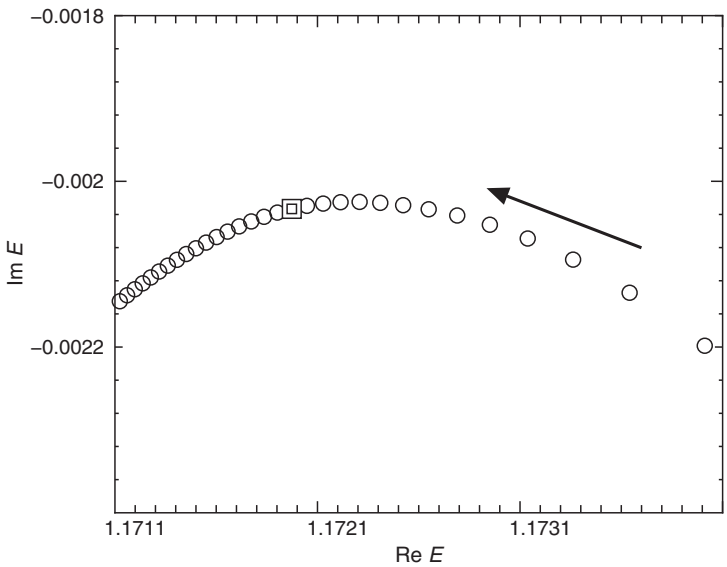

Fig. 11. Same as Fig. 9(b), but for the result calculated by the TG basis. See text for details.

The η trajectory calculated for the OG basis is shown in Fig. 10. Here the mesh of the trajectory is $\Delta\eta = 1.0\times10^{-6}$. In Fig. 10, we can observe the stationary series of the resonant eigenvalues around $\eta = \eta_{\rm o}^{\rm OG}$ (double square), which shows similar behavior to the SG trajectory in Fig. 9(b). In both the SG and OG trajectories, the sharp turning of the trajectory appears around the stationary region with the optimal $\eta_{\rm o}$, and the eigenvalue begins to move over a wide region if the strength goes beyond the optimal $\eta_{\rm o}$. In CSM, the resonance trajectory reveals slow-down behavior, in which a series of the eigenvalues settles almost into a stable point, if the number of basis functions is sufficient. In the ABC calculation, such slow-down behavior corresponds to the stationary behavior around the sharp turning, but the eigenvalues begin to leave the optimal point when the strength of the absorber is larger than its optimal value. This movement of the resonance is because a reflection effect from the

absorber becomes prominent. The resonance trajectory, being apart from the optimal point after the slow down, is also observed in the CSM calculation with an insufficient basis number [9,10].

Different behavior can be observed in the η trajectory of the TG basis, which is shown in Fig. 11. In this trajectory, the mesh of η is set to be $\Delta\eta = 1.0 \times 10^{-6}$. In the TG solution, there is no stationary and sharp turning behavior of the resonance around the optimal strength of η_o^{TG}, which is shown by the double square. We can see a monotonous increase of the level density around the double square. This monotonous variation is consistent with the broad minimum in the expectation value of the absorber, $\langle W(\eta)\rangle$, shown in Fig. 7. This broad minimum means that the resonance wave function is insensitive to the wide variation of the strength of the absorber around the optimal strength. This insensitivity is in contrast to the results of the SG and OG bases in Figs. 6 and 8, respectively, in which the sharp minimum points appear at the optimal strength.

4. Summary and discussion

In sum, we have applied the basis expansion method to a schematic two-body problem under the absorbing boundary condition. Three kinds of basis functions are employed: the shifted Gaussian (SG), the tempered Gaussian (TG), and the oscillating Gaussian (OG). The applicability of these Gaussian basis functions is explored by observing the complex eigenvalues, the wave functions, and the η dependence of the resonance eigenvalues.

First, we have focused on the properties of the energy eigenvalues of the continuum states, distributed in the complex energy plane. In the calculation by the SG basis, the distribution of the continuum eigenvalues is in accordance with an empirical sequence composed of the converged, indifferent, and diverging states. Moreover, not only the sharp resonance but also the broad resonance is clearly separated from the continuum states. In contrast, the distribution of the continuum states obtained by the TG basis deviates from the regular sequence. Some of the lower eigenvalues in the TG bases can follow the θ line of the converged states, but the deviation from the regular sequence is especially prominent in the indifferent states, which should have almost a constant value for the imaginary part. In the TG solutions, the maximum range is much more extended in comparison with the SG basis, but the broad resonance, which has a large imaginary part of the eigenvalue, is difficult to find in the complex energy plane. The OG calculation is successful in identifying the broad resonance, although the sequence of the non-resonant continuum deviates from the empirical regular sequence.

Secondly, we have compared the wave functions calculated by three kinds of basis functions. There is a strong basis dependence in the oscillation behavior of the wave functions. The non-resonant wave functions calculated from the SG basis strongly oscillate over a region of wide distance, and the amplitude of the non-resonant wave functions reaches a maximum at a distance far from the physical interaction region. The oscillation of the indifferent states is the most extensive of the three continuum states. The wave functions calculated from the TG bases cannot follow this extensive oscillation outside of the interaction region. The OG solutions can describe the extensive oscillation, although their main amplitudes are considerably localized at the inner region close to the physical interaction region.

Thirdly, we have investigated the expectation value of the absorbing potential, which is a measure of the error contained in the resonance wave function. In all the basis calculations, there is an optimal strength of the absorbing potential, which minimizes the error, and the small error is realized in the SG and OG bases. The η trajectory of the resonance is also observed in the complex energy plane.

The η trajectory in the SG and OG calculations reveals stationary behavior around the optimal η, but such stationary behavior does not appear in the trajectory of the TG calculation.

In view of the series of the present simple calculations, the shifted Gaussian is considered to be the most appropriate basis for the absorbing boundary condition. Of course, the basic feature of the oscillating Gaussian is the same as that for the shifted Gaussian and, hence, the oscillating Gaussian is also an applicable basis to the absorbing boundary condition. In the basis expansion method under the absorbing boundary condition, one of the errors arises from reflection by the absorber, which has a diverging property at an asymptotic region. To reduce the reflection from the diverging absorption, damping of the wave function must occur slowly as the distance increases. This slow damping requires that the basis functions are feasible enough to produce a broad and extensive oscillation of the wave function. Since a set of the shifted Gaussian is simply generated by shifting the peak position, a superposition of the shifted Gaussian can handle the wave function, which has an extensive oscillation over a region of wide distance. The present results justify the successful application of the ABC method to the microscopic cluster model, GCM, in which the shifted Gaussian naturally appears in a basis function [20,21].

In the present results, the tempered Gaussian seems to be inferior to the shifted and oscillating Gaussian bases. However, the tempered Gaussian itself is not necessarily inappropriate for the ABC method. In the variational calculation by the tempered Gaussian, there is a difficulty in generating the orthogonalized basis set, which is important in following the oscillating behavior over a wide region in the continuum wave function. As shown in the present analysis, the total number of the tempered Gaussian and its maximum range should be extended more than the calculation of the shifted and oscillating Gaussian, to generate a sufficient number of the orthogonalized basis sets. Thus, a pragmatic calculation employing the tempered Gaussian will be time-consuming in handling few-body systems.

In marked contrast to the present results for the absorbing boundary condition, the application of the tempered (and oscillating) Gaussian basis is successful in the complex scaling method [6,7]. In the complex scaling method, no asymptotic divergence in the matrix elements appears as long as the analytic properties of the physical interactions in the original Hamiltonian are not destroyed by the complex scaling. Thus, all the matrix elements of the physical interaction are safely damped in the asymptotic region. Moreover, in the complex scaling method with the tempered Gaussian, the scaling condition of $\mathbf{r} \to \mathbf{r}e^{i\theta}$ is transformed into the inverse scaling of the width parameter such as $\nu \to \nu e^{-2i\theta} = (\cos\theta - 2i\sin\theta)\nu$ [7]. Due to this inverse scaling, the tempered Gaussian has an oscillating feature, which is similar to the distribution of the oscillating Gaussian basis. Since the oscillating Gaussian can nicely describe the extensive oscillation around the interaction region, the scaled tempered [7] and oscillating [6] Gaussians are good trial functions for the complex scaling method.

Finally, we should comment on the application of the ABC method to few-body systems. In the present binary system, both the shifted Gaussian and oscillating Gaussian are successful in describing the resonance and continuum solutions. However, the oscillating Gaussian is superior to the shifted Gaussian if we consider the application of the ABC to few-body systems. In calculation of three-body systems, for instance, the coordinate rearrangements are essential to obtain the convergence of the total binding energy [1]. 2D integration appearing in the three-body matrix elements must be numerically performed if we handle the coordinate rearrangements by employing the shifted Gaussian basis. The multi-dimensional integration is quite time-consuming in few-body systems beyond three particles. In contrast, the oscillating Gaussian is a flexible basis for handling the coordinate rearrangements because the matrix elements with the rearrangements can be calculated

in an analytic manner [1]. Due to this flexibility, the oscillating Gaussian will be a pragmatic basis function in the few-body calculation under the absorbing boundary condition. We are now applying the ABC method to the three-body problem with coordinate rearrangements.

In conclusion, we should carefully consider a combination of trial functions and a boundary condition according to a kind of non-Hermitian transformation. It would be better to choose a type of trial function by considering the features of the non-Hermitian transformation. In the present analysis, we have mainly discussed the properties of the energy eigenvalues and their wave functions. However, a similar investigation of the basis dependence is interesting for the calculation of the strength function and the sum-rule value [7,11–14]. If we assume the extended completeness relation for the bound, resonant, and continuum states under the absorbing boundary condition, which has already been justified in the pragmatic calculations of the complex scaling method [7,12–14], we can easily calculate the strength function from the discretized solutions of the absorbing boundary condition. An analysis of the strength function and the extended completeness relation in the ABC method is now underway.

Acknowledgements

We thank Ms R. Kageyama and Mr M. Kudo, as well as all the members of the Theoretical Nuclear Physics laboratory at Kansai University for their useful discussions and kind support. One of the authors (M.I.) thanks Prof. H. G. Masui and T. Myo, and M. Kamimura for their careful reading of the manuscript, valuable comments, and useful discussions.

References

[1] E. Hiyama, Y. Kino, and M. Kamimura, Prog. Part. Nucl. Phys. **51**, 223 (2003).
[2] W. Horiuchi and Y. Suzuki, Phys. Rev. C **87**, 034001 (2013) and references therein.
[3] E. Hiyama and M. Kamimura, Phys. Rev. A **85**, 022502 (2012).
[4] E. Hiyama and M. Kamimura, Phys. Rev. A **85**, 062505 (2012).
[5] H. Horiuchi et al., Prog. Theor. Phys. Suppl. **62**, 1 (1977) and references therein.
[6] S. Ohtsubo, Y. Fukushima, M. Kamimura, and E. Hiyama, Prog. Theor. Exp. Phys. **7**, 073D02 (2013).
[7] S. Aoyama, T. Myo, K. Katō, and K. Ikeda, Prog. Theor. Phys. **116**, 1 (2006).
[8] Y. K. Ho, Phys. Rep. **99**, 1 (1983).
[9] A. T. Kruppa and K. Katō, Prog. Theor. Phys. **84**, 1145 (1990).
[10] T. Myo, K. Kato, and K. Ikeda, Phys. Rev. C **63**, 054313 (2001).
[11] M. Homma, T. Myo, and K. Kato, Prog. Theor. Phys. **97**, 561 (1997).
[12] T. Myo, A. Ohnishi, and K. Kato, Prog. Theor. Phys. **99**, 801 (1998).
[13] T. Myo and K. Kato, Prog. Phys. **98**, 1275 (1997).
[14] T. Myo, K. Kato, S. Aoyama, and K. Ikeda, Phys. Rev. C **63**, 054313 (2001).
[15] U. V. Riss and H.-D. Meyer, J. Phys. B **26**, 4503 (1993).
[16] U. V. Riss and H.-D. Meyer, J. Phys. B **28**, 1475 (1995).
[17] U. V. Riss and H.-D. Meyer, J. Phys. B **31**, 2279 (1998).
[18] S. Sahoo and Y. K. Ho, J. Phys. B **33**, 2195 (2000).
[19] S. Sahoo and Y. K. Ho, J. Phys. B **33**, 5151 (2000).
[20] M. Ito and K. Yabana, Prog. Theor. Phys. **113**, 1047 (2005).
[21] M. Ito, Phys. Lett. B **636**, 293 (2006).
[22] M. Ueda, K. Yabana, and T. Nakatsukasa, Phys. Rev. C **67**, 014606 (2003).
[23] T. Inakura, T. Nakatsukasa, and K. Yabana, Phys. Rev. C **80**, 044301 (2009).
[24] H. Masui and Y. K. Ho, Phys. Rev. C **65**, 054305 (2002).
[25] B. Gyaramati, K. T. Kuruppa, and K. F. Pal, Phys. Rev. A **41**, 3469 (1990).
[26] J.-Y. Ge and J. Z. H. Zhang, J. Chem. Phys. **108**, 1429 (1998).
[27] G. Jolicard, C. Leforestier, and E. J. Austin, J. Chem. Phys. **88**, 1026 (1988).